PERGAMON

International Journal of Solids and Structures 39 (2002) 4567–4582

INTERNATIONAL JOURNAL OF SOLIDS and STRUCTURES

www.elsevier.com/locate/ijsolstr

Piezolaminated beams with large deformations

A. Mukherjee *, A. Saha Chaudhuri

Department of Civil Engineering, Indian Institute of Technology, Bombay, Mumbai 400076, India

Received 30 April 2001; received in revised form 22 March 2002

Abstract

The objective of the present paper is to demonstrate the effect of large deformations on the piezoelectric materials and structures. An energy based electromechanical piezoelectric constitutive law derived by Tiersten is adopted. For large deformation analysis of beams a counterpart of Von Karman's plate equation is considered. The displacement fields in finite element method are based on the first order shear deformation theory. To analyze the nonlinear equilibrium equations an incremental iterative technique based on the Newton–Raphson method is employed. In the present algorithm the equilibrium is examined considering the electromechanical coupling effects. Nonlinear effects due to transverse and axial loading on a cantilever and a pinned–pinned PVDF bimorph beam have been investigated.

Keywords: Piezoelectric materials; Large deformation; Newton–Raphson method; Stress stiffening; Stress softening

1. Introduction

The concept of piezoelectric smart materials and structural systems with highly integrated sensors and actuators has led to a revolution in controlling the behavior of complex flexible structures. For low mass and highly flexible structures geometric nonlinear effects due to large deformations cannot be ignored. To control such a structure an accurate estimation of voltage sensed by the piezoelectric sensors is necessary to provide the exact remedial actuation voltage. However, research on large deformation of piezolaminated structures is scanty. Faria and Almedia (1999) worked on the enhancement of prebuckling behavior of composite beams with geometric imperfections using piezoelectric actuators. Thompson and Loughlan (1995) carried out experimental studies on the active buckling control of some composite column strips using piezo ceramic actuators. Icardi and Sciuva (1996) presented large deflection and stress analysis of multilayered plates with induced strain actuators. Reddy (1999) presented a formulation on laminated composite plates with integrated sensors and actuators including large deformations. Chandrashekhara and Bhatia (1993) presented a finite element analysis for active buckling of smart composite plates. Kalyanraman (1999) presented a review of smart instability control of struts. Gaudenzi and Bathe (1995) presented an iterative finite element procedure for the analysis of piezoelectric continua including electromechanical

* Corresponding author. Tel.: +91-22-578-2545; fax: +91-22-578-3480.
E-mail address: abhijit@civil.iitb.ac.in (A. Mukherjee).

0020-7683/02/$ - see front matter
PII: S0020-7683(02)00341-4

coupling. Oh et al. (2000) studied postbuckling and vibration characteristics of piezolaminated composite plate subject to thermopiezoelectric loads. They also worked on the thermopiezoelastic snapping of piezolaminated plates using layerwise nonlinear finite elements (2001).

In this paper, we present a generalized formulation for large deformation of piezoelectric structures that includes the electromechanical coupling. In the proposed algorithm Newton–Raphson method is used to check the equilibrium equations at every iteration (Crisfield, 1991). Large deformation problems due to transverse and axial loading have been investigated for a PVDF bimorph beam.

2. Piezoelectric constitutive relations

Based on the energy principles that include electrical as well as elastic effects, Tiersten (1969) presented the simplified version of linear piezoelectric constitutive equations. These equations for the kth layer of a piezolaminated structure are:

$$\text{Direct effect:} \quad \mathbf{D}_k = \mathbf{e}_k \boldsymbol{\varepsilon}_k + \boldsymbol{\xi}_k \mathbf{E}_k \tag{1}$$

$$\text{Converse effect:} \quad \boldsymbol{\sigma}_k = \overline{\mathbf{Q}}_k \boldsymbol{\varepsilon}_k - \mathbf{e}_k^t \mathbf{E}_k \tag{2}$$

where $\mathbf{D}$ is the electric displacement vector, $\mathbf{e}$, piezoelectric stress coefficient matrix, $\boldsymbol{\xi}$, dielectric constant matrix, $\mathbf{E}$, electric field vector, $\boldsymbol{\varepsilon}$, mechanical strain vector, $\boldsymbol{\sigma}$, mechanical stress vector, $\overline{\mathbf{Q}}$, matrix of elastic constants.

As direct and converse piezoelectric effects are electromechanically coupled, the voltage induced in the sensor actuates the structure as well. The actuation force $(\mathbf{e}_{31}\mathbf{E}_3^k)$ is added to the mechanical stress vector $\boldsymbol{\sigma}_x$. Therefore, after each iteration the load vector requires modification. The modified load vector, in turn, changes the voltage sensed. An iterative process evolves where we look for the convergence of the sensed voltage and the deflection.

When the piezoelectric material is poled in thickness direction only Eq. (2) can be written as follows (Eisenberger and Abramovich, 1997):

$$\begin{Bmatrix} \sigma_x \\ \sigma_y \\ \tau_{yz} \\ \tau_{xz} \\ \tau_{xy} \end{Bmatrix}_k = \begin{bmatrix} Q_{11} & Q_{12} & 0 & 0 & Q_{16} \\ Q_{12} & Q_{22} & 0 & 0 & Q_{26} \\ 0 & 0 & Q_{44} & Q_{45} & 0 \\ 0 & 0 & Q_{45} & Q_{55} & 0 \\ Q_{16} & Q_{26} & 0 & 0 & Q_{66} \end{bmatrix}_k \begin{Bmatrix} \varepsilon_x \\ \varepsilon_y \\ \gamma_{yz} \\ \gamma_{xz} \\ \gamma_{xy} \end{Bmatrix}_k - \begin{bmatrix} 0 & 0 & e_{31} \\ 0 & 0 & e_{31} \\ 0 & e_{15} & 0 \\ 0 & e_{15} & 0 \\ 0 & 0 & 0 \end{bmatrix}_k \begin{Bmatrix} 0 \\ 0 \\ E_3 \end{Bmatrix}_k \tag{3}$$

For the beam problem σ_y, τ_{yz} and τ_{xy} are zero. Therefore, Eq. (3) reduces to,

$$\begin{Bmatrix} \sigma_x \\ \tau_{xz} \end{Bmatrix}_k = \begin{bmatrix} \overline{Q}_{11} & 0 \\ 0 & \overline{Q}_{55} \end{bmatrix}_k \begin{Bmatrix} \varepsilon_x \\ \gamma_{xz} \end{Bmatrix}_k - \begin{bmatrix} e_{31} \\ 0 \end{bmatrix}_k E_3^k \tag{4}$$

where the relation for $\overline{Q}_{ij}$ in terms of Q_{ij} are given by

$$\overline{Q}_{11} = Q_{11} + \left(\frac{Q_{16}Q_{26} - Q_{12}Q_{66}}{Q_{22}Q_{66} - Q_{26}^2} \right) Q_{12} + \left(\frac{Q_{12}Q_{26} - Q_{22}Q_{66}}{Q_{22}Q_{66} - Q_{26}^2} \right) Q_{16} \tag{5}$$

$$\overline{Q}_{55} = Q_{55} - \frac{Q_{45}^2}{Q_{44}} \tag{6}$$

The displacement field is based on the first order shear deformation theory

$$U = u_0 - z\theta_y; \quad W = w_0 \tag{7}$$

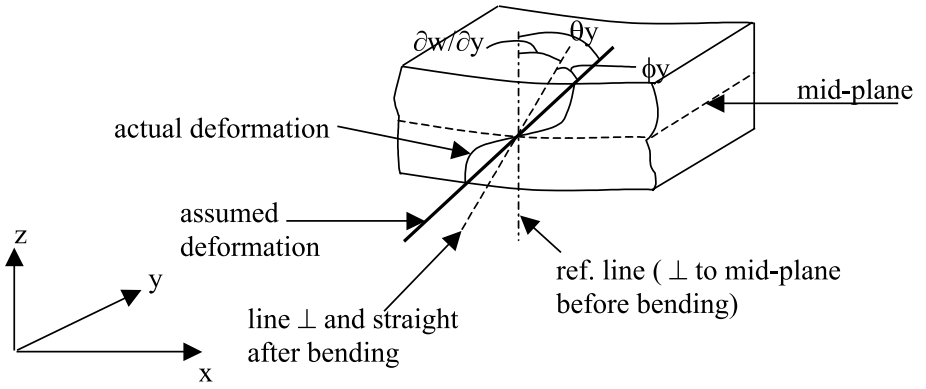

Fig. 1. Assumption of shear deformation over beam thickness.

At a distance 'z' from the reference plane the strains at any point can be expressed as

$$\begin{Bmatrix} \varepsilon_x \\ \gamma_{xy} \end{Bmatrix} = \begin{Bmatrix} \dfrac{\partial U}{\partial x} \\ \dfrac{\partial U}{\partial z} + \dfrac{\partial W}{\partial x} \end{Bmatrix} = \begin{Bmatrix} \dfrac{\partial u_0}{\partial x} - z\dfrac{\partial \theta_y}{\partial x} \\ -\theta_y + \dfrac{\partial w_0}{\partial x} \end{Bmatrix} = \begin{Bmatrix} \dfrac{\partial u_0}{\partial x} - z\dfrac{\partial \theta_y}{\partial x} \\ \phi \end{Bmatrix} \tag{8}$$

where u_0 and w_0 are the in plane and the transverse displacements at the reference plane (i.e. midplane) respectively and θ_y is the rotation of transverse normal about y-axis (Fig. 1).

3. Geometric nonlinearity

The mathematical formulation for geometrically nonlinear static analysis is based on the virtual work equations for a continuum within a total Lagrange co-ordinate system. Von Karman's large deflection theory is adopted here. For a continuum undergoing displacements the equation of equilibrium of the external and the internal forces are expressed as (Zeinkiewicz, 1971):

$$\boldsymbol{\psi} = \int_L \mathbf{B}^{\mathrm{T}}\boldsymbol{\sigma}\,\mathrm{d}A - \mathbf{P} = \mathbf{0} \tag{9}$$

where $\boldsymbol{\psi}$ is the sum of internal and external generalized forces, $\mathbf{B}$ is the strain–displacement matrix that includes both linear and nonlinear components and $\mathbf{P}$ is the generalized nodal force vector.

Now, expressing $\boldsymbol{\sigma}$ in terms of rigidity matrix $\mathbf{D}$, the strain–displacement matrix $\mathbf{B}$ and the nodal displacement vector $\boldsymbol{\delta}$, the governing equation (9) can be written as

$$\mathbf{K}_{\mathrm{S}}\boldsymbol{\delta} = \mathbf{P} \tag{10}$$

where $\mathbf{K}_{\mathrm{S}}$ is the secant stiffness matrix, $\boldsymbol{\delta}$ is the nodal displacement vector and $\mathbf{P}$ is the force vector. An incremental equation is required to solve this set of nonlinear equations that can be written as

$$\mathbf{K}_{\mathrm{T}}\,\mathrm{d}\boldsymbol{\delta} = \mathrm{d}\mathbf{P} \tag{11}$$

where $\mathbf{K}_{\mathrm{T}}$ is the tangent stiffness matrix, $\mathrm{d}\boldsymbol{\delta}$ and $\mathrm{d}\mathbf{P}$ are increments of displacement and force vectors respectively.

We shall now develop the linear stiffness matrix $\mathbf{K}_0$, the secant stiffness matrix $\mathbf{K}_{\mathrm{S}}$ and the tangent stiffness matrix $\mathbf{K}_{\mathrm{T}}$.

3.1. Linear stiffness matrix

A three node isoparametric beam element is considered here. The quadratic variation of displacement function for bending and membrane element can be written as

$$U = \sum_{i=1}^{3} N_i u_i; \quad W = \sum_{i=1}^{3} N_i w_i; \quad \theta_y = \sum_{i=1}^{3} N_i \theta_{yi} \tag{12}$$

where N_i is Lagrangian quadratic shape function of the ith node of the beam.

Using Eq. (8) the strains at any point in the beam can be expressed in terms of those at the mid-plane

$$\begin{Bmatrix} \varepsilon_x \\ \gamma_{xz} \end{Bmatrix} = \begin{bmatrix} 1 & z & 0 \\ 0 & 0 & 1 \end{bmatrix} \begin{Bmatrix} \dfrac{\partial u_0}{\partial x} \\ -\dfrac{\partial \theta_y}{\partial x} \\ \phi \end{Bmatrix} = \mathbf{H}\bar{\boldsymbol{\varepsilon}}_0 \tag{13}$$

where $\mathbf{H}$ is the transformation matrix of individual lamina strain to that in the reference plane. After transforming the strains to the reference plane of the laminated beam, we can write the element linear stiffness matrix using the principle of virtual work as follows:

$$\mathbf{K}_0 = \int_v \mathbf{B}_0^{\mathrm{T}} \mathbf{H}^{\mathrm{T}} \overline{\mathbf{Q}} \mathbf{H} \mathbf{B}_0 \, \mathrm{d}v = \int_L \mathbf{B}_0^{\mathrm{T}} \overline{\mathbf{D}} \mathbf{B}_0 \, \mathrm{d}x \tag{14}$$

where $\overline{\mathbf{D}} = b \int_h \mathbf{H}^{\mathrm{T}} \overline{\mathbf{Q}} \mathbf{H} \, \mathrm{d}z$ and b is the width of the beam.

3.2. Nonlinear stiffness matrix

The nonlinear strain–displacement relationship is based on Pica et al. (1980). The additional strain produced by the large deformation effect is expressed at the following reference-plane strain vector:

$$\bar{\boldsymbol{\varepsilon}} = \begin{Bmatrix} \dfrac{\partial u_0}{\partial x} \\ -\dfrac{\partial \theta_y}{\partial x} \\ \phi \end{Bmatrix} + \begin{Bmatrix} \dfrac{1}{2}\left(\dfrac{\partial u_0}{\partial x}\right)^2 + \dfrac{1}{2}\left(\dfrac{\partial w_0}{\partial x}\right)^2 \\ 0 \\ 0 \end{Bmatrix} = \bar{\boldsymbol{\varepsilon}}_0 + \bar{\boldsymbol{\varepsilon}}_L \tag{15}$$

where, $\bar{\boldsymbol{\varepsilon}}_0 = \mathbf{B}_0 \boldsymbol{\delta}$ are linear strain components as described earlier

$$\bar{\boldsymbol{\varepsilon}}_L = \begin{Bmatrix} \dfrac{1}{2}\left(\dfrac{\partial u_0}{\partial x}\right)^2 + \dfrac{1}{2}\left(\dfrac{\partial w_0}{\partial x}\right)^2 \\ 0 \\ 0 \end{Bmatrix} = \frac{1}{2} \begin{bmatrix} \dfrac{\partial u_0}{\partial x} & \dfrac{\partial w_0}{\partial x} \\ 0 & 0 \\ 0 & 0 \end{bmatrix} \begin{Bmatrix} \dfrac{\partial u_0}{\partial x} \\ \dfrac{\partial w_0}{\partial x} \end{Bmatrix} = \frac{1}{2} \mathbf{A} \bar{\boldsymbol{\varepsilon}}_n$$

$$\mathbf{A}^{\mathrm{T}} = \begin{bmatrix} \dfrac{\partial u_0}{\partial x} & 0 & 0 \\ \dfrac{\partial w_0}{\partial x} & 0 & 0 \end{bmatrix} \quad \text{and} \quad \bar{\boldsymbol{\varepsilon}}_n = \mathbf{G}\boldsymbol{\delta}; \quad \text{where} \quad \mathbf{G} = \begin{bmatrix} \dfrac{\partial N_i}{\partial x} & 0 & 0 \\ 0 & \dfrac{\partial N_i}{\partial x} & 0 \end{bmatrix} \quad i = 1, 2, 3$$

The variation of generalized strain vector given by Eq. (15) with respect to $\mathrm{d}\boldsymbol{\delta}$ can be written as

$$\mathrm{d}\bar{\boldsymbol{\varepsilon}} = \mathrm{d}\bar{\boldsymbol{\varepsilon}}_0 + \mathrm{d}\bar{\boldsymbol{\varepsilon}}_L$$

Using FE discretization it can be written as

$$\bar{\boldsymbol{\varepsilon}} = \left(\mathbf{B}_0 + \frac{1}{2}\mathbf{B}_L\right)\boldsymbol{\delta}; \quad \mathrm{d}\bar{\boldsymbol{\varepsilon}} = (\mathbf{B}_0 + \mathbf{B}_L)\,\mathrm{d}\boldsymbol{\delta} = \mathbf{B}\,\mathrm{d}\boldsymbol{\delta}$$

where $\mathbf{B}_L = \mathbf{A}\mathbf{G}$.

3.3. Tangent stiffness matrix

In Newton–Raphson solution technique, the derivative of nonlinear equations is obtained by taking the variation of the equilibrium equations. The equilibrium equations are defined by Eq. (9). The variation of the above equations can be written as

$$\mathrm{d}\boldsymbol{\psi} = \int_L \mathrm{d}\mathbf{B}^{\mathrm{T}}\boldsymbol{\sigma}\,\mathrm{d}x + \int_L \mathbf{B}^{\mathrm{T}}\,\mathrm{d}\boldsymbol{\sigma}\,\mathrm{d}x - \mathrm{d}\mathbf{P} \tag{16}$$

This incremental equation can be expressed as

$$\mathrm{d}\boldsymbol{\psi} = \mathbf{K}_{\mathrm{T}}\,\mathrm{d}\boldsymbol{\delta} - \mathrm{d}\mathbf{P} \tag{17}$$

where $\mathbf{K}_{\mathrm{T}}$ is the tangential stiffness matrix of the beam element and is given by,

$$\mathbf{K}_{\mathrm{T}} = \mathbf{K}_0 + \mathbf{K}_L + \mathbf{K}_\sigma \tag{18}$$

where $\mathbf{K}_0$ is the linear stiffness matrix,$\mathbf{K}_L$ is the large displacement stiffness matrix,

$$\int_L \mathbf{B}_0^{\mathrm{T}}\overline{\mathbf{D}}\mathbf{B}_L\,\mathrm{d}x + \int_L \mathbf{B}_L^{\mathrm{T}}\overline{\mathbf{D}}\mathbf{B}_0\,\mathrm{d}x + \int_L \mathbf{B}_L^{\mathrm{T}}\overline{\mathbf{D}}\mathbf{B}_L\,\mathrm{d}x \tag{19}$$

$\mathbf{K}_\sigma$ is the geometric stiffness matrix,

$$\int_L \mathbf{G}^{\mathrm{T}}\mathbf{S}_0\mathbf{G}\,\mathrm{d}x + \int_L \mathbf{G}^{\mathrm{T}}\mathbf{S}_L\mathbf{G}\,\mathrm{d}x \tag{20}$$

where $\mathbf{S}_0$ and $\mathbf{S}_L$ are linear and nonlinear axial stresses in the element.

3.4. Secant stiffness matrix

Using the stress strain relationship the equilibrium equations can be written as

$$\int_L \mathbf{B}^{\mathrm{T}}\overline{\mathbf{D}}\bar{\boldsymbol{\varepsilon}}\,\mathrm{d}x = \mathbf{P}$$

The above equation can be rewritten as

$$\int_L (\mathbf{B}_0 + \mathbf{B}_L)^{\mathrm{T}}\overline{\mathbf{D}}\left(\mathbf{B}_0 + \frac{1}{2}\mathbf{B}_L\right)\mathrm{d}x\boldsymbol{\delta} = \mathbf{P} \tag{21}$$

Therefore, the secant stiffness is

$$\mathbf{K}_{\mathrm{S}} = \int_L \mathbf{B}_0^{\mathrm{T}}\overline{\mathbf{D}}\mathbf{B}_0\,\mathrm{d}x + \frac{1}{2}\int_L \mathbf{B}_0^{\mathrm{T}}\overline{\mathbf{D}}\mathbf{B}_L\,\mathrm{d}x + \int_L \mathbf{B}_L^{\mathrm{T}}\overline{\mathbf{D}}\mathbf{B}_0\,\mathrm{d}x + \frac{1}{2}\int_L \mathbf{B}_L^{\mathrm{T}}\overline{\mathbf{D}}\mathbf{B}_L\,\mathrm{d}x \tag{22}$$

This secant stiffness matrix is unsymmetrical. For direct iteration technique this matrix can be converted into a symmetric one (Wood and Schrefler, 1978). Alternatively, we can find the equilibrated mechanical force vector using the equilibrium equations at every iteration. Subtracting the equilibrated force vector from the initial incremental force vector the unequilibrated force vector can be determined. The second method has been used in the present formulation.

3.5. Solution procedure

For solution of nonlinear equations several procedures are available viz. incremental procedure, stepwise procedure and iterative procedure. Among the available solution procedures, the Newton–Raphson

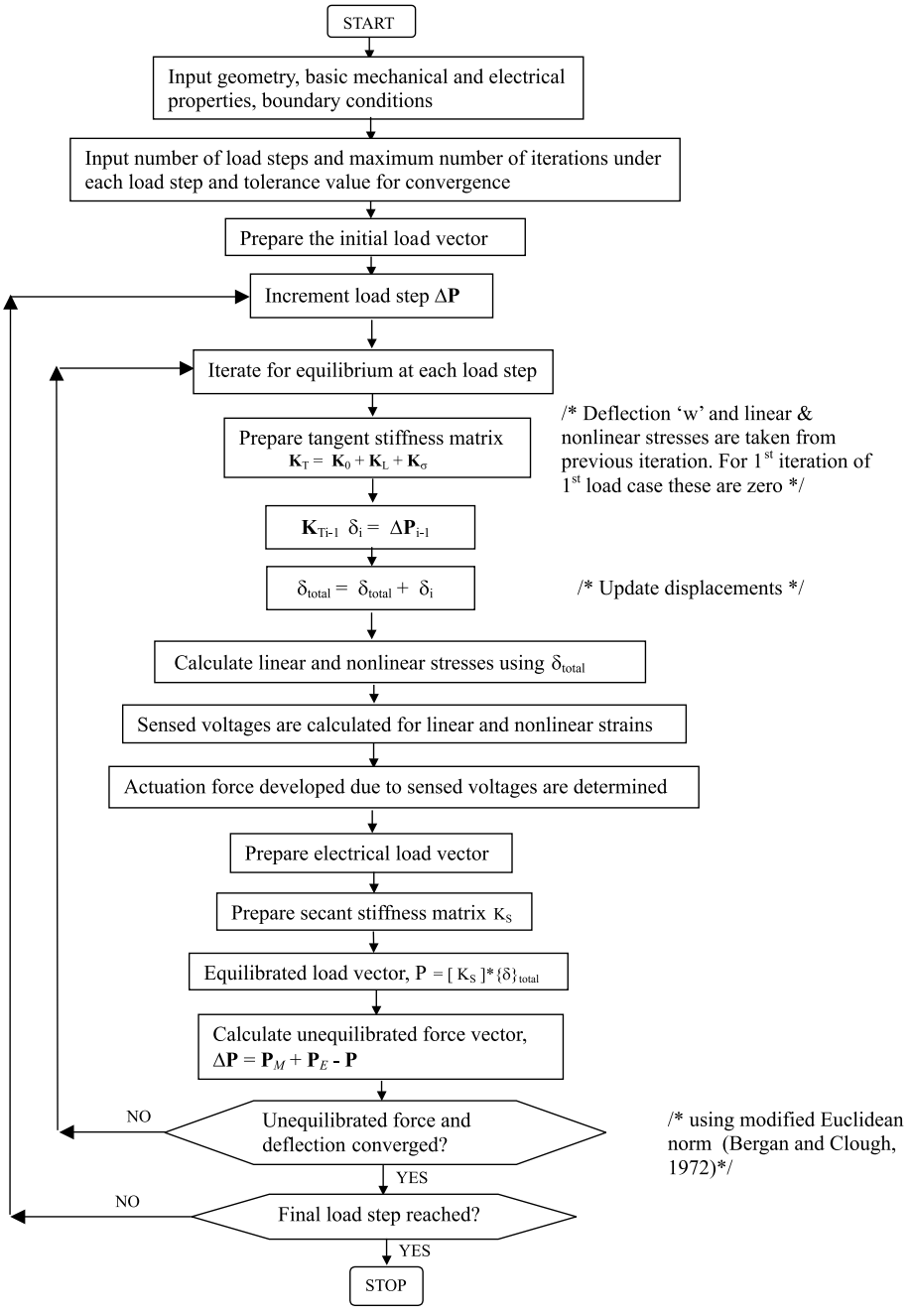

Fig. 2. Flow diagram.

method, that is an incremental iterative method, is a commonly used technique to solve large deformation problems. One limitation of the method is that it cannot handle snap through phenomenon. The snap through can be solved by the arc-length method (Oh et al., 2001). In the present paper, Newton–Raphson method has been adopted to solve the nonlinear static equilibrium equations. In the present solution the equilibrium condition can be written as

$$\mathbf{K}_S\boldsymbol{\delta} = \mathbf{P}_M + \mathbf{P}_E \tag{23}$$

where $\mathbf{P}_M$ and $\mathbf{P}_E$ are the mechanical and electrical load vectors respectively. The electrical load vector is a function of the deformation of the structure. Therefore, $\mathbf{P}_E$ is updated iteratively at each load step.

It may be noted in equation (23) that the displacement vector $\boldsymbol{\delta}$ does not contain the electrical displacement and the electrical load vector $\mathbf{P}_E$ has been calculated separately. However, the iterative nature (Fig. 2) of the solution of equation (23) allows us to maintain the electromechanical coupling. The electrical load vector is updated at each iteration based on the voltage sensed. Therefore, using equation (23) the convergence of both unequilibrated voltages, forces and deflections is achieved. The convergence is based on the Euclidean norm (Bergan and Clough, 1972) and the tolerance is taken as 0.0001. Fig. 2 illustrates the solution procedure.

4. Numerical examples

To validate the developed algorithm a number of problems have been solved. This paper focuses on the large deformation effects on sensing and actuation phenomenon of PVDF bimorphs. The dimensions of the beam used in all the examples are shown in Fig. 3 and the material properties for PVDF are given in Table 1.

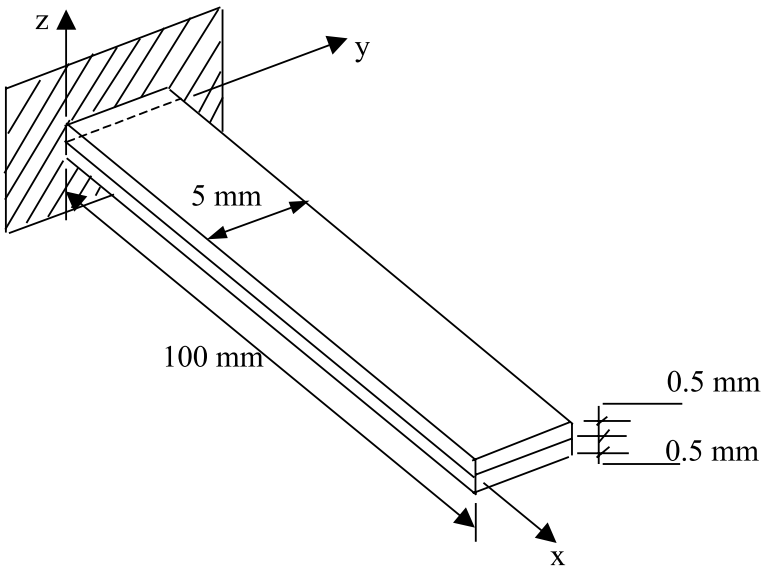

Fig. 3. PVDF bimorph.

Table 1
Properties of PVDF

Elastic constant, E ($\mathrm{N\,m^{-2}}$)	2.0×10^9
Poisson's ratio, v	0.29
Density, ρ ($\mathrm{kg\,m^{-3}}$)	1800
Piezoelectric stress coefficient, e_{31} ($\mathrm{C\,m^{-2}}$)	0.046
Dielectricity, ξ_{33} ($\mathrm{F\,m^{-1}}$)	0.1062×10^{-9}
Maximum operating voltage ($\mathrm{V\,\mu m^{-1}}$)	30

Table 2
Comparison of results for piezo bimorph cantilever beam

PL^2/EI	$(\Delta/L)_{\text{nonlinear}}$ (Fertis, 1993)	$(\Delta/L)_{\text{nonlinear}}$ (present)	$(\Delta/L)_{\text{linear}}$
1.11	0.33	0.35	0.37
5.55	0.73	0.75	1.85
13.88	0.84	0.87	4.63
16.66	0.86	0.88	5.55
27.77	0.89	0.91	9.25
55.55	0.92	0.93	18.50

4.1. Example 1

In this example the large deformation effect in the bimorph cantilever beam due to transverse load at its tip is investigated. The deflection ratios (Δ/L) for different values of load ratio (PL^2/EI) are presented in Table 2. Here Δ is the tip deflection, L is the length of the beam, P is the tip load and EI is the flexural rigidity. The results corroborate well with those given by Fertis (1993) (Table 2). The results of linear analysis are presented to highlight the divergence between the linear and nonlinear responses with increasing load. The results suggest that the sensed voltages would also be significantly different in nonlinear case as compared to the linear case. This effect is examined in the subsequent examples.

4.2. Example 2

A cantilever PVDF bimorph shown in Fig. 3 is subjected to unit voltage in the transverse direction. In the present work, the effect of electromechanical coupling is taken into account. It is observed that the results for an uncoupled and coupled system do not vary significantly (Fig. 4). The present results also compare well with the linear prediction of Tzou (1993) and analytical results.

Due to applied voltage the deflection in the beam is small. Thus, geometric nonlinear effect in the structure is negligible. However, the nonlinear effect can be significant in presence of other mechanical forces in the system. We shall examine this point in the next example.

4.3. Example 3

To examine the large deformation effect on sensed voltage of a cantilever bimorph, a varying transverse force upto 0.5 N ($PL^2/EI = 6$) is applied at the free end. For this load linear analysis predicts a deflection ratio 2.00. However, due to the stress-stiffening effect in the nonlinear analysis it reduces to 0.76 (Fig. 5).

The sensors can be used in two configurations—patch or continuous. In continuous sensors, the cumulative charge collected over the entire domain is obtained. In patch sensors, on the other hand, the charge collected in each patch is available. Therefore, a spatial variation of voltage can be obtained in patch sensors. Fig. 6 shows the distribution of sensed voltage over entire length of the beam. In this case it is

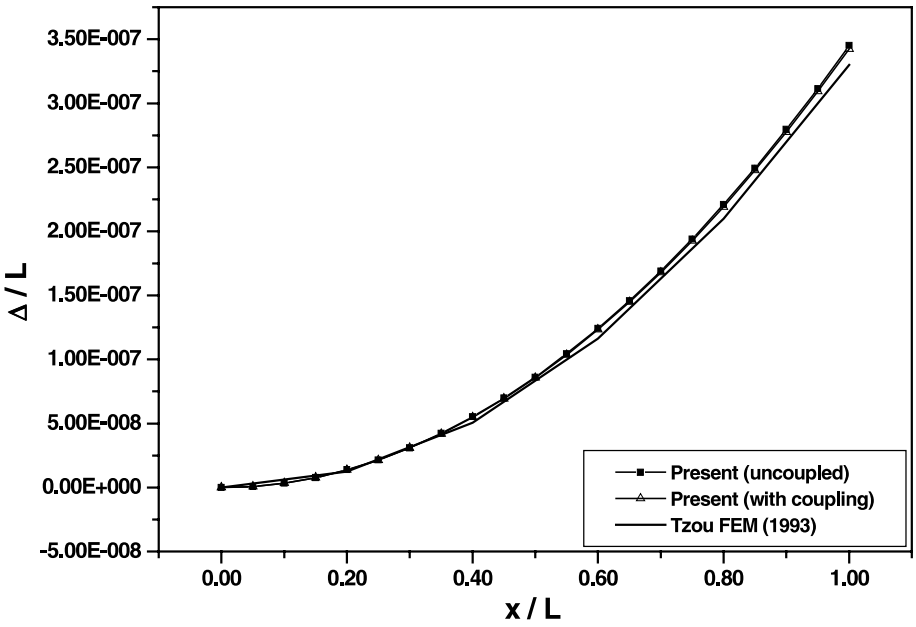

Fig. 4. Nodal deflections of cantilever piezo bimorph due to unit voltage.

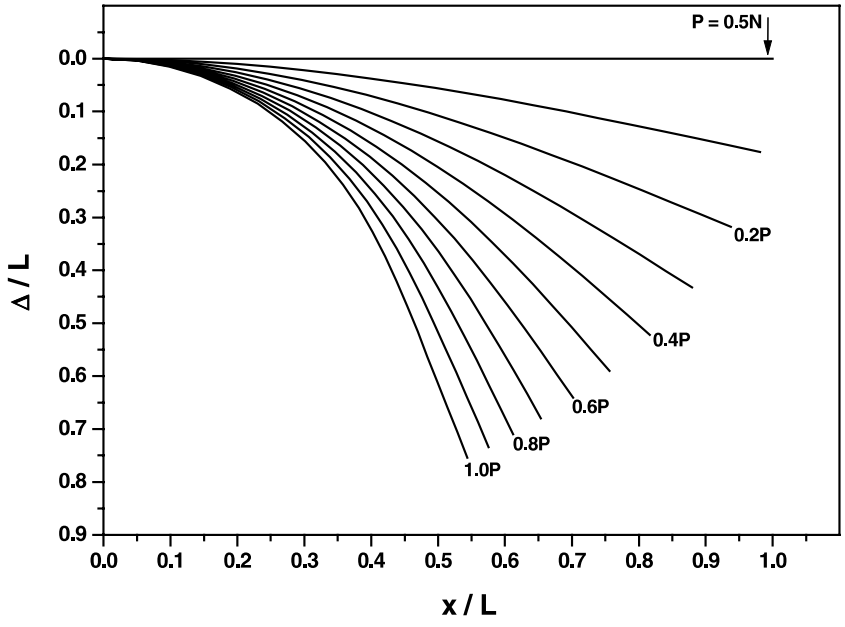

Fig. 5. Deflected shape at various load steps.

noticed that concentration of voltage near the fixed end is very high compared to that at the free end. In comparison, the linear analysis predicts a linear variation of voltage. It also overpredicts the voltage to a large extent. Fig. 7 shows the sensor voltage at the root of the cantilever beam due to an increasing tip

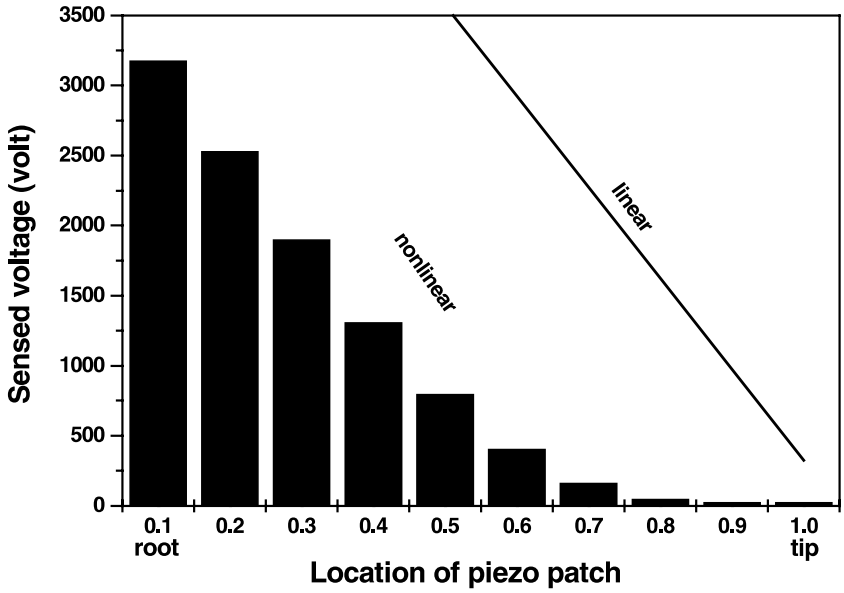

Fig. 6. Distribution of sensed voltages along the beam at final load step.

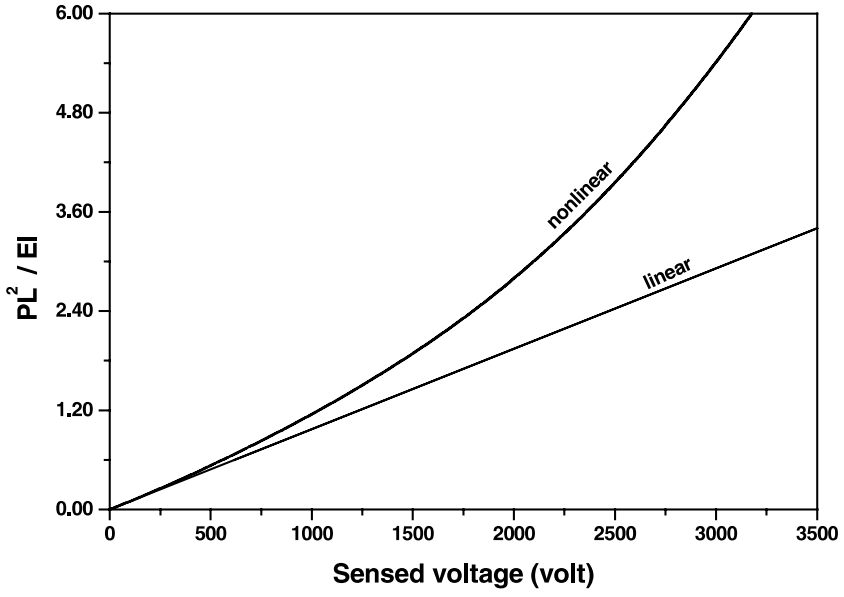

Fig. 7. Sensed voltage developed at fixed end.

transverse load up to 0.5 N. The voltage sensed in the linear and the nonlinear cases has been compared. As the load ratio grows the two graphs diverge rapidly. As a result the voltage sensed by the piezoelectric material is significantly less than the sensed voltage predicted through linear analysis.

4.4. Example 4

In the previous example we investigated the stress stiffening for a purely transverse load. The stiffening effect is more predominant when the load is applied at an oblique angle. To study this effect the cantilever bimorph is subjected to a tip load of 0.5 N acting at an angle 45° with vertical. In the present case the deflection ratio at the maximum load is 0.46 as against 1.4 in case of linear analysis and 0.65 in case of nonlinear analysis only due to transverse component of inclined load (Fig. 8). Here stress-stiffening effect occurs due to combined action of the horizontal and the vertical component of the load. The voltage distribution in the present case is also markedly different (Fig. 9) from the previous case (Fig. 6). The axial force induced in the structure considerably reduces the voltages developed in the sensor (Fig. 10) as compared to the previous case (Fig. 7).

In this case tip deflection reduces at higher rate as the horizontal component of the applied load and axial force developed due to nonlinear strain are additive. However, if the inclination of load is in the opposite direction, then the axial force will negate the nonlinear strain effect, thus reducing the difference between the linear and nonlinear results.

4.5. Example 5

In this example the nonlinear variation of sensed voltage due to the structural indeterminacy in the system is investigated. A PVDF bimorph with both ends pinned is subjected to a transverse load of 0.05 N at the midpoint as shown in Fig. 11. The material properties and dimensions are presented in Table 1 and Fig. 3. Fig. 12 highlights the nonlinear effects due to stress stiffening in the structure. Accordingly, the sensed voltage is significantly less than that of linear analysis (Fig. 13).

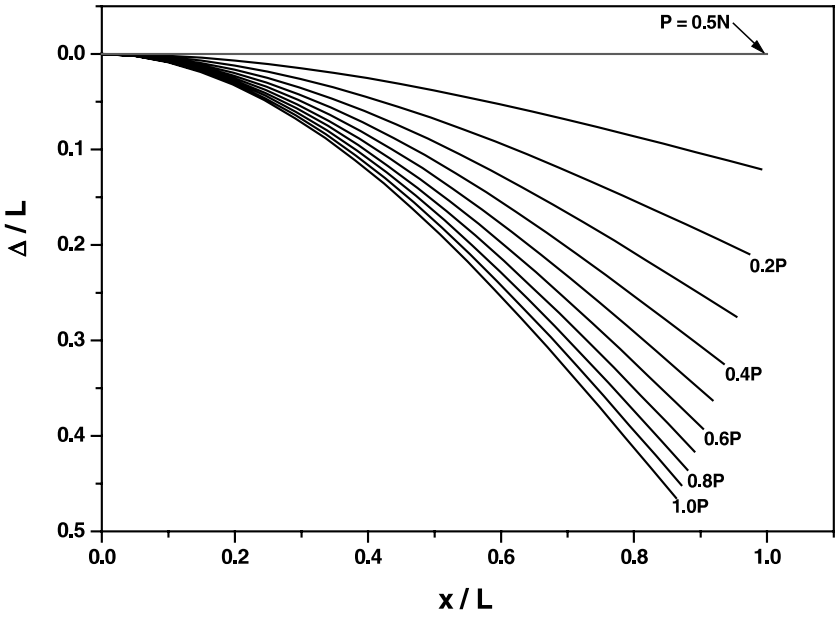

Fig. 8. Deflected shape at various load steps.

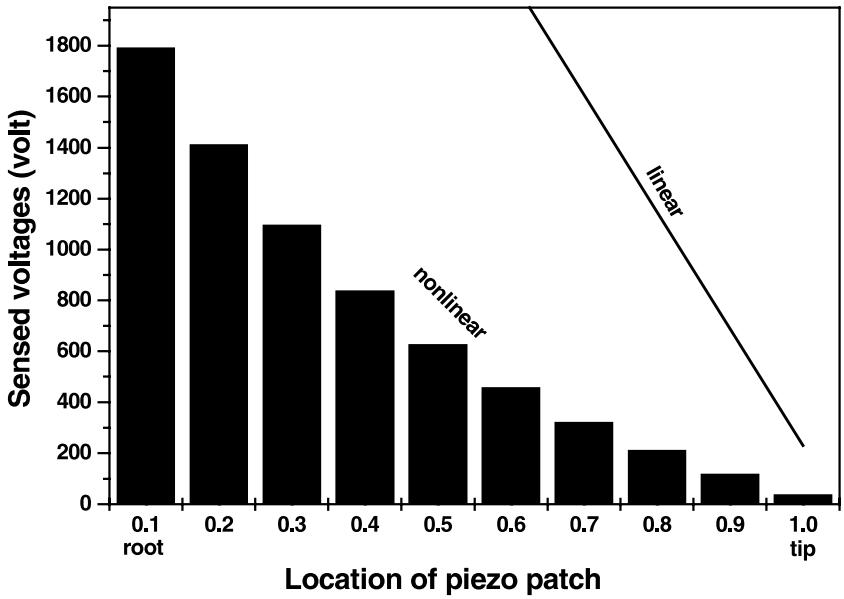

Fig. 9. Distribution of sensed voltages along the beam at final load.

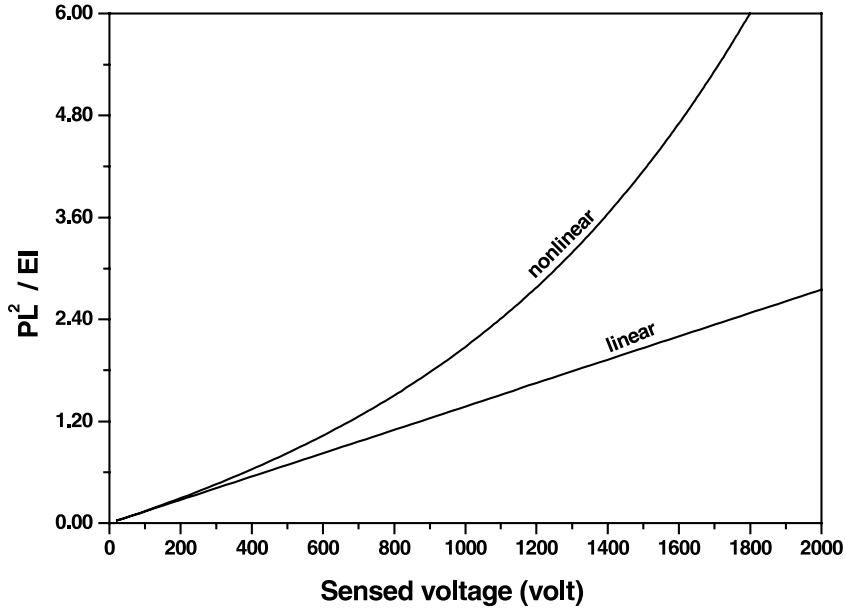

Fig. 10. Sensed voltage at fixed end.

4.6. Example 6

In the previous examples we obtained the effects of geometric nonlinearity that leads to stiffening of the system. As a result, the voltage developed in the structure is less than that for the linear analysis. In this

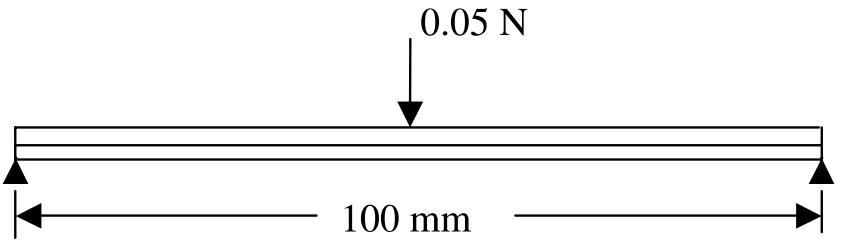

Fig. 11. Both end pinned bimorph with transverse load at midpoint.

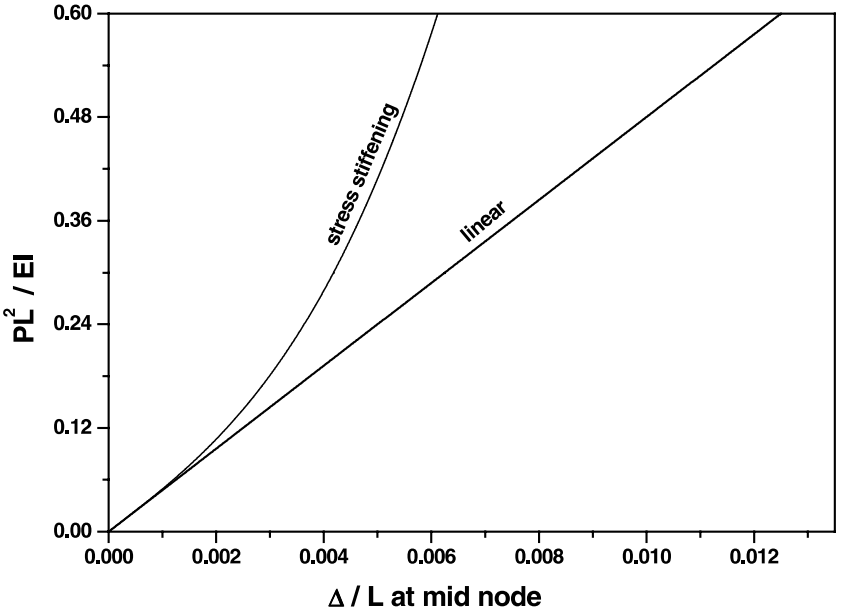

Fig. 12. Load vs deflection at midnode.

example, we explore the situations where geometric nonlinearity leads to reduction of the stiffness of the structure. The response of the cantilever bimorph under axial compressive load is investigated along with a small transverse tip load to trigger the transverse deflection. A 0.025 N transverse load with 0.1 N axial load is applied. The deflection ratio due to linear analysis is 0.10. Due to stress softening in nonlinear analysis it increases to around 0.20 (Fig. 14). The generation of sensed voltage at the root is also nonlinear in nature as shown in Fig. 15. In the stress softening case the sensed voltage generated is much higher than the linear analysis. As a result the required remedial actuation voltage is also higher than that in the linear analysis.

4.7. Example 7

In the previous examples, we presented the results for sensing in a PVDF bimorph. In this example, the actuation is demonstrated. The cantilever bimorph with an axial compressive force at the tip is supplied with a voltage from an external source. The applied voltage is varied from 200 to 1400 V. It is seen in Fig. 16 that in presence of actuation voltage axial compressive force results in large transverse deformations. The transverse deformation for increasing axial load converges asymptotically to the bifurcation load of the

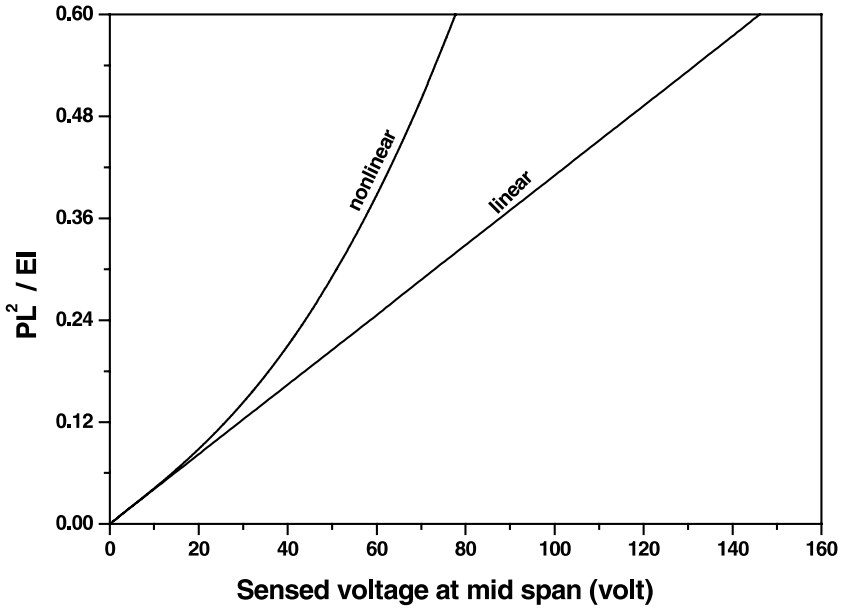

Fig. 13. Nonlinear variation of sensed voltage.

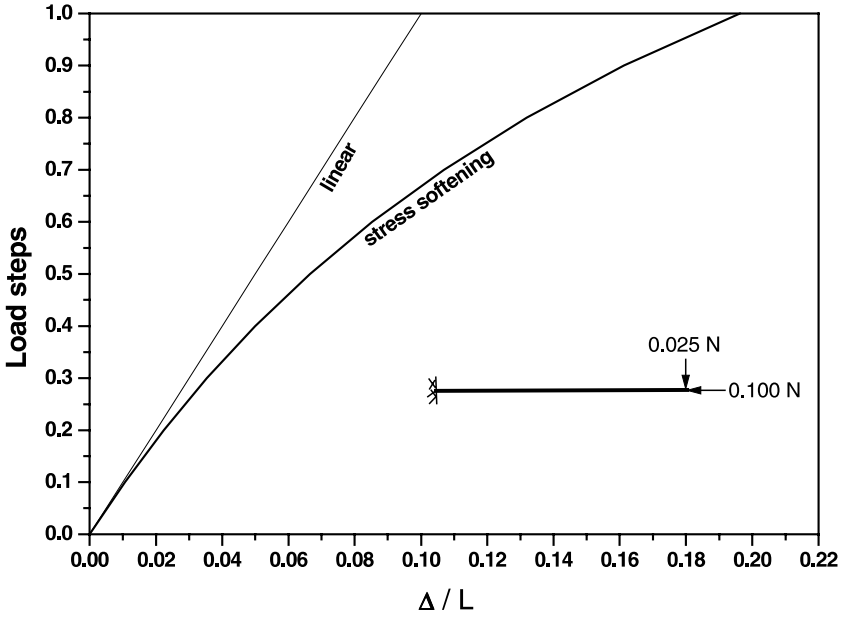

Fig. 14. Stress softening effect on tip deflection due to axial compressive loading.

straight column. In presence of an actuation the structure does not display bifurcation and it generates a finite transverse deflection for all levels of loads. This result highlights the importance of approaching a buckling problem as a nonlinear problem in which prebuckling deformations due to actuation are present.

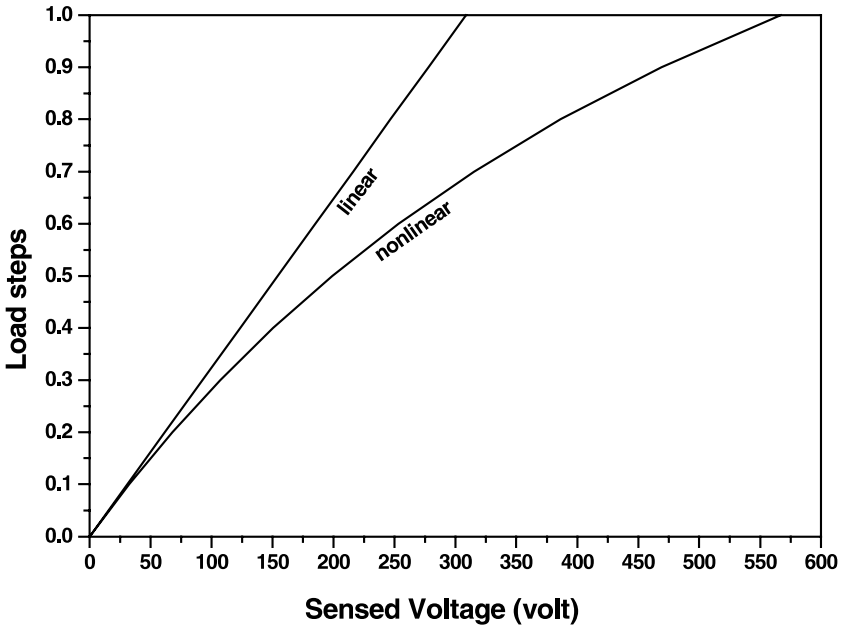

Fig. 15. Variation of sensed voltage at fixed end.

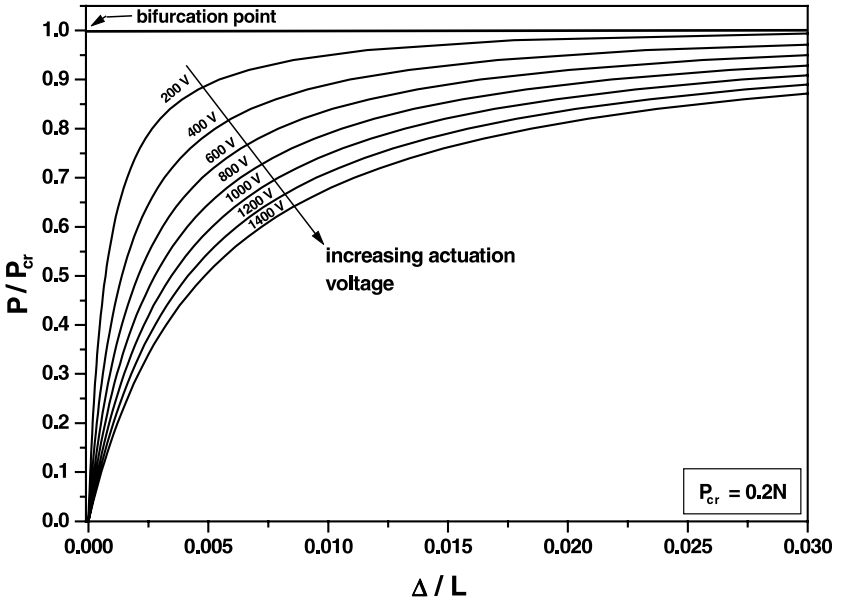

Fig. 16. Transverse deflection of strut with initial actuation.

It is also possible to remedy the initial imperfections in a strut by applying actuations that counter the imperfection.

5. Closing remarks

The geometric nonlinear analysis of piezolaminated beams has been presented. The nonlinear effects greatly alter the response of piezoelectric materials. In stress-stiffening case, sensed voltage in nonlinear analysis is significantly less than that obtained from linear analysis. The stress stiffening may occur due to the development of large tensile forces in the structure caused by either large deformations or structural indeterminacy. In stress softening, on the other hand, the sensed voltage is higher than that obtained from linear analysis. Therefore, to administer an exact remedial actuation to control such structures one must consider the nonlinear effects on the sensed voltage.

In the present work, the electromechanical coupling is also incorporated. However, in all the cases it has been observed that the coupling effect is not predominant.

The presence of actuation along with axial compressive force generates finite transverse deflections. The deflection asymptotically approaches infinity with the axial force approaching the buckling load. The results highlight the importance of nonlinear effects in flexible piezolaminated structures.

Acknowledgements

The authors thankfully acknowledge the suggestions of Dr. A. Samanta, Ship Surveyor, Research and Co-ordination Division, Indian Register of Shipping.

References

Bergan, P.G., Clough, R.W., 1972. Convergence criteria for iterative process. AIAA Journal 10 (8), 1107–1108.

Chandrashekhara, K., Bhatia, K., 1993. Active buckling control of smart composite plates—finite element analysis. Smart Materials and Structures 2, 31–39.

Crisfield, M.A., 1991. In: Nonlinear Finite Element Analysis of Solids and Structures, vol. 1. John Wiley and Sons Ltd, England.

Eisenberger, M., Abramovich, H., 1997. Shape control of non-symmetric piezolaminated composite beams. Composite Structures 38 (1–4), 565–571.

Faria, A.R.De., Almedia, F.M.De., 1999. Enhancement of pre-buckling behavior of composite beams with geometric imperfections using piezoelectric actuators. Composites: Part B 30, 43–50.

Fertis, D.G., 1993. Nonlinear Mechanics. CRC Press Inc, Florida.

Gaudenzi, P., Bathe, K.J., 1995. An iterative finite element procedure for the analysis of piezoelectric continua. Journal of Intelligent Materials Systems and Structures 6, 266–273.

Icardi, U., Sciuva, M.Di., 1996. Large-deflection and stress analysis of multilayered plates with induced-strain actuators. Smart Materials and Structures 5, 140–164.

Kalyanraman, V., 1999. Smart control of instability of struts. In: Proceedings of the International Conference on Smart Materials, Structures and Systems. Allied Publishers, New Delhi.

Oh, I.K., Han, J.H., Lee, I., 2000. Postbuckling and vibration characteristics of piezolaminated composite plate subject to thermo-piezoelectric loads. Journal of Sound and Vibration 233 (1), 19–40.

Oh, I.K., Han, J.H., Lee, I., 2001. Thermopiezoelastic snapping of piezolaminated plates using layerwise nonlinear finite elements. AIAA Journal 39 (6), 1188–1198.

Pica, A., Wood, R.D., Hinton, E., 1980. Finite element analysis of geometrically nonlinear plate behaviour using a Mindlin formulation. Computers and Structures 11, 203–215.

Reddy, J.N., 1999. On laminated composite plates with integrated sensors and actuators. Engineering Structures 21, 568–593.

Thompson, S.P., Loughlan, J., 1995. The active buckling control of some composite column strips using piezoceramic actuators. Composite Structures, 32, 59–67.

Tiersten, H.F., 1969. Linear piezoelectric plate vibrations. Plenum (New York).

Tzou, H.S., 1993. Piezoelectric shells—distributed sensing and control of continua. Kluwer Academic Publishers, Netherlands.

Wood, R.D., Schrefler, B., 1978. Geometrically nonlinear analysis—a correlation of finite element notations. International Journal for Numerical Methods in Engineering 12, 635–642.

Zeinkiewicz, O.C., 1971. The finite element method in engineering science. McGraw-Hill, London.